Click Here for Full Article

Statistical maritime radar duct estimation using hybrid genetic algorithm–Markov chain Monte Carlo method

Caglar Yardim,[1,2] Peter Gerstoft,[2] and William S. Hodgkiss[1,2]

[1] This paper addresses the problem of estimating the lower atmospheric refractivity (M profile) under nonstandard propagation conditions frequently encountered in low-altitude maritime radar applications. This is done by statistically estimating the duct strength (range- and height-dependent atmospheric index of refraction) from the sea surface reflected radar clutter. These environmental statistics can then be used to predict the radar performance. In previous work, genetic algorithms (GA) and Markov chain Monte Carlo (MCMC) samplers were used to calculate the atmospheric refractivity from returned radar clutter. Although GA is fast and estimates the maximum a posteriori (MAP) solution well, it poorly calculates the multidimensional integrals required to obtain the means, variances, and underlying posterior probability distribution functions of the estimated parameters. More accurate distributions and integral calculations can be obtained using MCMC samplers, such as the Metropolis-Hastings and Gibbs sampling (GS) algorithms. Their drawback is that they require a large number of samples relative to the global optimization techniques such as GA and become impractical with an increasing number of unknowns. A hybrid GA-MCMC method based on the nearest neighborhood algorithm is implemented in this paper. It is an improved GA method which improves integral calculation accuracy through hybridization with a MCMC sampler. Since the number of forward models is determined by GA, it requires fewer forward model samples than a MCMC, enabling inversion of atmospheric models with a larger number of unknowns.

1. Introduction

[2] In many maritime regions of the world, such as the Mediterranean, Persian Gulf, East China Sea, and California Coast, atmospheric ducts are common occurrences. They result in various anomalies such as significant variations in the maximum operational radar range and increased sea clutter. Hence radar systems operating in these environments would benefit from knowing the effects of the environment on their system performance. This requires knowledge of the atmospheric refractivity, which is usually represented by the modified refractivity (M profile) in the radar community [see *Skolnik*, 2001].

[3] Evaporation and surface-based ducts are associated with increased sea clutter due to the heavy interaction between the sea surface and the electromagnetic signal trapped within the duct. However, this unwanted clutter is a rich source of information about the environment and can be used to determine the local atmospheric conditions. This can be a valuable addition to other more conventional techniques such as radiosondes, rocket-sondes, microwave refractometers and meteorological models such as the Coupled Ocean/Atmospheric Meso-scale Prediction System (COAMPS) that give M profile forecasts [*Rowland and Babin*, 1987; *Thews*, 1990; *Hodur*, 1996; *Skolnik*, 2001]. In a Bayesian framework, the results of one or several of these techniques and regional duct statistics [*Babin*, 1996] can be coupled with the clutter inversion to improve the overall estimation quality. An attractive feature of inferring refractivity

---

[1]Electrical and Computer Engineering Department, University of California, San Diego, La Jolla, California, USA.
[2]Marine Physical Laboratory, Scripps Institution of Oceanography, University of California, San Diego, La Jolla, California, USA.
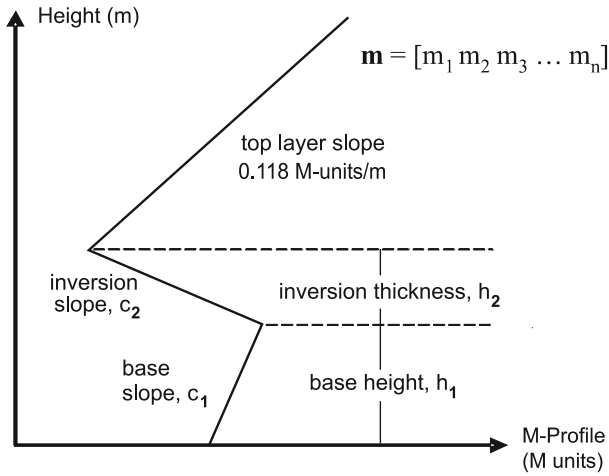
Figure 1. Four-parameter range-independent trilinear M profile.

from sea surface clutter is that it does not use additional hardware or extra meteorological/electromagnetic measurements. It extracts the information from the radar clutter obtained during normal radar operation, which usually is readily available both as a function of range, direction and time. For a fast inversion algorithm, a near-real-time M profile structure is obtained. The need for a fast algorithm that updates the environmental estimates at intervals of 30 min or less is evident in work by *Rogers* [1996], where the RMS error in propagation factor exceeds 6 dB after 30 min because of temporal decorrelation.

[4] Various techniques that estimate the M profile using radar clutter return are proposed by *Rogers et al.* [2000], *Gerstoft et al.* [2003,2004], *Barrios* [2004], *Rogers et al.* [2005], *Yardim et al.* [2006], and *Vasudevan et al.* [2007]. Most of these refractivity from clutter (RFC) techniques use an electromagnetic fast Fourier transform (FFT) split-step parabolic equation (SSPE) approximation to the wave equation [*Barrios*, 1994; *Levy*, 2000], whereas some also make use of ray-tracing techniques. While the paper by *Rogers et al.* [2000] exclusively deals with evaporation duct estimation, other techniques are applicable to both evaporation, surface-based and mixed type of ducts that contain both an evaporation section and an surface-based type inversion layer. *Vasudevan et al.* [2007] exploits the inherent Markovian structure of the FFT parabolic equation approximation and uses a particle filtering approach, whereas *Barrios* [2004] uses rank correlation with ray tracing to estimate the M profile.

[5] In contrast, *Gerstoft et al.* [2003, 2004] and *Yardim et al.* [2006] use global parameterization within a Bayes-

ian framework. Since the unknown model parameters are defined as random variables in a Bayesian framework, the inversion results will be in terms of the means, variances and marginal, as well as the *n*-dimensional joint posterior probability distributions, where *n* represents the number of unknown duct parameters. This gives the user not only the ability to obtain the maximum a posteriori (MAP) solution, but also the prospect of performing statistical analysis on the inversion results and the means to convert these environmental statistics into radar performance statistics. These statistical calculations can be performed by taking multidimensional integrals of the joint probability distribution functions (PPD). *Gerstoft et al.* [2003] use genetic algorithms to estimate the MAP solution. However, no statistical analysis is performed since classical genetic algorithms (GA) are not suitable for the necessary integral calculations. While *Gerstoft et al.* [2004] use importance sampling, *Yardim et al.* [2006] use Markov chain Monte Carlo (MCMC) samplers to perform the MC integration [*Ó Ruanaidh and Fitzgerald*, 1996; *MacKay*, 2003]. Although they provide the means to quantify the impact of uncertainty in the estimated duct parameters, they require large numbers of forward model runs and hence they lack the speed to be near-real-time methods and are not suitable for models with large numbers of unknowns.

[6] In this paper, a hybrid GA-MCMC technique is implemented. The method reduces the number of forward model runs required to perform the RFC inversion, while still being able to perform MC integration. It is first tested on the synthetic data used by [*Yardim et al.* [2006] with a four-parameter, range-independent, trilinear M profile model (Figure 1). Then data collected during the 1998 Wallops Island experiment (Wallops'98) [see *Gerstoft et al.*, 2003] are analyzed using a 16-parameter range-dependent atmospheric model to show the capabilities and limitations of the method. An evaporative duct structure is not appended in this work but it can be done by introducing a Jeske-Paulus (JP) [*Jeske*, 1973; *Paulus*, 1985] or Liu-Katsaros-Businger (LKB) [*Liu et al.*, 1979] profile using one or more extra evaporation duct parameters, depending on the conditions.

2. Model Formulation

[7] For electromagnetic propagation purposes, the environment can be uniquely represented by the range and height-dependent index of refraction, which itself is a complex function of temperature, humidity, and pressure [*Cook and Burk*, 1992]. Therefore the term environmental parameters will be used exclusively for the M profile parameters henceforth. To formulate the problem, a classical Bayesian framework is adopted, where the M profile model and the radar measured sea surface clutter data are denoted by the vectors **m** and **d**, respectively. An

electromagnetic FFT-SSPE is used to propagate the field in an environment given by $\mathbf{m}$ and obtain synthetic clutter returns $f(\mathbf{m})$. Since the unknown environmental parameters m are assumed to be random variables, the solution to the inversion is given by their joint posterior probability distribution function (PPD or p($\mathbf{m}|\mathbf{d}$)). Bayes' formula can be used to write the PPD as

$$p(\mathbf{m}|\mathbf{d}) = \frac{\mathcal{L}(\mathbf{m})p(\mathbf{m})}{\int_{\mathbf{m}'} \mathcal{L}(\mathbf{m}')p(\mathbf{m}')d\mathbf{m}'}, \tag{1}$$

where p($\mathbf{m}$) is the prior probability distribution function (pdf) of the parameters. Any information obtained from other methods and regional duct statistics can be incorporated in this step as a prior belief. Since this paper investigates the ability to infer M profiles using RFC, a uniform prior is used. However, it is possible to include statistical meteorological priors from studies such as that of *Babin* [1996], for some of the parameters (e.g., the duct height).

[8] Assuming a zero-mean Gaussian error between the measured and modeled clutter, the likelihood function is given by

$$\mathcal{L}(\mathbf{m}) = (2\pi)^{-N_\mathrm{R}/2}|\mathbf{C_d}|^{-1/2}$$
$$\times \exp\left[-\frac{(\mathbf{d}-f(\mathbf{m}))^\mathrm{T}\mathbf{C_d}^{-1}(\mathbf{d}-f(\mathbf{m}))}{2}\right], \tag{2}$$

where $\mathbf{C_d}$ is the data error covariance matrix, $(\cdot)^\mathrm{T}$ is the transpose and N_R is the number of range points used (length of the data vector, $\mathbf{d}$). Further simplification can be achieved by assuming that the errors are spatially uncorrelated with identical distribution for each data point forming the vector $\mathbf{d}$. For this case, $\mathbf{C_d} = \nu\mathbf{I}$, where ν is the variance and $\mathbf{I}$ the identity matrix. Then the equation can be simplified to

$$\mathcal{L}(\mathbf{m}) = (2\pi\nu)^{-N_\mathrm{R}/2}\exp\left[-\frac{\phi(\mathbf{m})}{2\nu}\right], \tag{3}$$

where

$$\phi(\mathbf{m}) = (\mathbf{d}-f(\mathbf{m}))^\mathrm{T}(\mathbf{d}-f(\mathbf{m})). \tag{4}$$

[9] The maximum likelihood (ML) estimate for the error variance can be found by solving $\partial\mathcal{L}/\partial\nu = 0$, which results in

$$\hat{\nu}_{ML} = \frac{\phi(\mathbf{m})}{N_\mathrm{R}}. \tag{5}$$

[10] After inserting it back into the likelihood function, $\mathcal{L}(\mathbf{m})$ finally can be reduced to

$$\mathcal{L}(\mathbf{m}) = \left[\frac{N_\mathrm{R}}{2\pi e\phi(\mathbf{m})}\right]^{N_\mathrm{R}/2} \tag{6}$$

$$p(\mathbf{m}|\mathbf{d}) \propto p(\mathbf{m})\left[\frac{N_\mathrm{R}}{2\pi e\phi(\mathbf{m})}\right]^{N_\mathrm{R}/2}. \tag{7}$$

[11] Having defined the posterior density, any statistical information about the unknown environmental and radar parameters can now be calculated by taking these multidimensional integrals:

$$\mu_i = \int \ldots \int m_i'p\left(\mathbf{m}'|\mathbf{d}\right)d\mathbf{m}' \tag{8}$$

$$\sigma_i^2 = \int \ldots \int \left(m_i' - \mu_i\right)^2 p\left(\mathbf{m}'|\mathbf{d}\right)d\mathbf{m}' \tag{9}$$

$$p(m_i|\mathbf{d}) = \int \ldots \int \delta\left(m_i' - m_i\right)p\left(\mathbf{m}'|\mathbf{d}\right)d\mathbf{m}', \tag{10}$$

where μ_i, σ_i^2, p($m_i|\mathbf{d}$) are posterior means (Bayesian minimum mean square error (MMSE) estimate), variances, and marginal PPDs of M profile parameters.

[12] Probability distributions of parameters of interest to a radar operator are calculated in a similar fashion. Assume that u is such a parameter of interest (e.g., propagation factor), which naturally is some function $u = g(\mathbf{m})$ of the radar environment m. A statistical analysis of u can be carried out by transformation of random variables. The classical transformation formula

$$p(u|\mathbf{d}) = \frac{p(\mathbf{m}|\mathbf{d})}{|J(\mathbf{m})|}, \tag{11}$$

where $J(\mathbf{m})$ represents the Jacobian of the transformation, can be written in integral form [*Huang et al.*, 2006]

$$p(u|\mathbf{d}) = \int \ldots \int \delta\left(u - g\left(\mathbf{m}'\right)\right)p\left(\mathbf{m}'|\mathbf{d}\right)d\mathbf{m}', \tag{12}$$

in the same form as (8)–(10). This form is preferred since it enables the evaluation of desired quantities with MC integration.

3. Hybrid GA-MCMC Method

[13] To improve the lack of accuracy in GA and lack of speed in MCMC, a hybrid method based on the nearest neighborhood algorithm (NA) [*Sambridge*, 1999a,

1999b, 2001, 2003] is adopted here. This method effectively converts the samples gathered during a typical global optimization run (e.g., GA) into a form that can be used in MC integration. Then it uses a fast MCMC to compute these integrals.

3.1. Monte Carlo Integration and Genetic Algorithms

[14] Notice that all of the integrals in (8)–(10) and (12) are of the form

$$I = \int g(x)p(x)dx, \qquad (13)$$

where x is a random variable with a pdf of $p(x)$, and $g(x)$ is some function of x. These multidimensional integrals can be estimated numerically using the Monte Carlo integration technique [Ó Ruanaidh and Fitzgerald, 1996]. Assuming a large number of random x values are drawn from a sampling distribution $p_s(x)$, $\{x^1, x^2, x^3, \ldots, x^{N_s}\}$, the integral I can be estimated as

$$I \simeq \frac{\sum_{i=1}^{N_s} \frac{p(x^i)g(x^i)}{p_s(x^i)}}{\sum_{i=1}^{N_s} \frac{p(x^i)}{p_s(x^i)}}. \qquad (14)$$

[15] By introducing a weight function the integral can be approximated as

$$w(x^i) \triangleq \frac{p(x^i)}{p_s(x^i)}, \qquad (15)$$

$$I \simeq \frac{\sum_{i=1}^{N_s} w(x^i)g(x^i)}{\sum_{i=1}^{N_s} w(x^i)}. \qquad (16)$$

[16] This is the well known importance sampling formula, where $p_s(x)$ is usually selected to be a uniform or Gaussian density. The main drawback of this approach is the slow convergence and relatively low accuracy resulting from the difference between the parameter pdf $p(x)$ and the sampling pdf $p_s(x)$. The best result is obtained if $p_s(x) = p(x)$, which is used by MCMC techniques such as Metropolis-Hastings [Metropolis et al., 1953; Hastings, 1970] and Gibbs samplers [Geman and Geman, 1984].

[17] Importance sampling is used for RFC inversion by Gerstoft et al. [2004], where the prior $p(\mathbf{m})$ is used as the sampling density. However, the results depend on how close $p(\mathbf{m})$ is to $p(\mathbf{m}|\mathbf{d})$. Both Metropolis and Gibbs samplers are used by Yardim et al. [2006] with $p_s(\mathbf{m}) = p(\mathbf{m}|\mathbf{d})$. A drawback of these techniques is the necessity to run many forward modeling runs. Many global optimizers such as the classical GA do not have a

$p_s(x)$. Every run will result in a different distribution concentrated around the higher-density regions. However, because of its speed, it is desirable to use GA in MC integration. Such an approach requires a technique that estimates the integrals (8)–(10) and (12) using an ensemble of GA samples without a $p_s(x)$.

3.2. Voronoi Decomposition

[18] A sampling density $p_s(x)$ that is an approximation to $p(\mathbf{m}|\mathbf{d})$, is created using the information gathered from the ensemble of GA samples. Then this approximate PPD $\widehat{p}(\mathbf{m}|\mathbf{d})$ is used to calculate the Bayesian integrals by replacing (15)–(16) with

$$w(\mathbf{m}^i) = \frac{p(\mathbf{m}^i|\mathbf{d})}{\widehat{p}(\mathbf{m}^i|\mathbf{d})} \simeq 1 \qquad (17)$$

$$I \simeq \frac{1}{N_S} \sum_{i=1}^{N_s} g(\mathbf{m}^i). \qquad (18)$$

Here $\widehat{p}(\mathbf{m}|\mathbf{d})$ is obtained by using Voronoi decomposition (or Dirichlet tessellation) of the n-dimensional model space [Voronoi, 1908; Okabe et al., 2000]. It creates a convex n-dimensional polytope (a polygon if $n = 2$, a polyhedron if $n = 3$) called a Voronoi cell (or Dirichlet domain) around the nearest neighborhood of each GA point. For a given set of GA samples there exists a unique set of corresponding Voronoi cells that tessellates the model space. This structure is adaptable and if points are changed, removed or added, the cells rearrange themselves, shrink and enlarge to reflect the changes. Therefore, even if the ensemble of GA samples change with every independent simulation, Voronoi lattice will adjust and likely provide accurate Bayesian integral calculations.

[19] For nearest neighborhood calculations a weighted L_2 norm is used to compute the distances. The weight removes the units of the parameters, specifically between the M layer slopes (M units/m) and layer thicknesses (m). If available, the prior model covariance matrix can be used as the norm weight. Since no a priori information is used, the weight is only used to scale each parameter so that all parameters lie within $[0, 1]$ range, contributing equally to norm calculations. Therefore, with an initial set of GA samples $\{\mathbf{m}^1, \mathbf{m}^2, \mathbf{m}^3, \ldots, \mathbf{m}^{N_{GA}}\}$ without a $p_s(\mathbf{m})$,

$$\left\| \mathbf{m} - \mathbf{m}^i \right\|_W^2 = \left(\mathbf{m} - \mathbf{m}^i\right)^T W \left(\mathbf{m} - \mathbf{m}^i\right) \qquad (19)$$

$$V_i = \left\{ \mathbf{m} : i = \arg \min_{i'} \left\| \mathbf{m} - \mathbf{m}^{i'} \right\|_W \right\} \qquad (20)$$

$$\widehat{p}(\mathbf{m} \in V_i|\mathbf{d}) = p(\mathbf{m}^i|\mathbf{d}), \qquad (21)$$

where W is the weight and V_i is the ith Voronoi cell centered at the ith GA sample $\mathbf{m}^i$. $\widehat{p}(\mathbf{m}|\mathbf{d})$ is constant inside the cell, effectively discretizing the original PPD into N_{GA} possible levels. Similar to an A/D converter, it will convert the true "analog" PPD into a "digitized" approximation. The only difference is that, this A/D converter is n dimensional, and hence discrete levels are n-dimensional polytopes.

[20] With this assumption, $\widehat{p}(\mathbf{m}|\mathbf{d})$ is known at any point anywhere in the entire search space and there is no need for any further forward model runs.

3.3. MCMC (Gibbs) Resampling

[21] Now that a sampling density $p_s(\mathbf{m}) = \widehat{p}(\mathbf{m}|\mathbf{d})$ is defined, the next step is drawing samples from this PPD to compute (18) for any desired function $g(\cdot)$. Unlike classical MCMC, this MCMC sampler will not suffer from the high number of forward model runs required for MCMC because it operates on the approximate PPD, requiring no forward modeling.

[22] The perfect MCMC sampler for this task is the Gibbs sampler (GS) [*Geman and Geman*, 1984; *Ó Ruanaidh and Fitzgerald*, 1996; *Yardim et al.*, 2006] and is also used in the neighborhood algorithm [*Sambridge*, 1999b]. Therefore the term GS will be used instead of the MCMC henceforth. GS gets samples by updating one parameter at a time in a circulatory fashion and it uses the local conditional one-dimensional (1-D) PPD to update each parameter. After all of the parameters are updated once, the result will form the next Gibbs sample. This is a particularly fast algorithm since the Metropolis acceptance/rejection criterion used in MCMC samplers is always met and every proposed point is accepted. The difficulty is that, it requires the knowledge of conditional 1-D PPDs, which often are not available for many inversion problems. However, here the conditional is available via Voronoi cells.

[23] A simple example in Figure 2 illustrates the approach with only two unknown parameters. Voronoi cells are constructed around each GA sample (stars) to create the approximate PPD where $\widehat{p}(\mathbf{m}|\mathbf{d})$ is constant in each polygon. To obtain the next Gibbs sample (diamonds) first the local 1-D conditional probability density is calculated along the line intersecting the original Gibbs sample. The local conditional density $p(m_1|m_2, \mathbf{d})$ for the first Gibbs sample (PPD along AA′) is plotted above the Voronoi diagram. Since the conditional PPD only changes at the cell boundaries, computation of the intersection points with AA′ is sufficient to extract the local PPD. This lets us use the Voronoi decomposition without actually having to estimate the Voronoi cell structures or calculate their vertices. Afterward, a sample is drawn from this simple 1-D PPD and the parameter m_1 is updated accordingly. To complete the cyclic updating of each parameter, parameter m_2 is also updated using the

local conditional PPD $p(m_2|m_1, \mathbf{d})$ (PPD along BB′), plotted on the right-hand side of the Voronoi diagram.

[24] The intersection between Voronoi cells and the conditional line is calculated using the procedure given by *Sambridge* [1999a]. Two neighboring Voronoi cells V_i and V_j intersecting the conditional line are given in Figure 3. They are created around their corresponding cell centers (GA samples m^i and m^j) and Gibbs sampler is updating along the kth axis by sampling from $\widehat{p}(m_k|\forall m_l\ l \neq k, \mathbf{d})$. The boundary can be calculated using the fact that the distances from both cell centers m^i and m^j to the boundary point b^{ij} must be same by the definition of nearest neighborhood. Hence using W = I,

$$\left\|\mathbf{m}^i - \mathbf{b}^{ij}\right\|^2 = \left\|\mathbf{m}^j - \mathbf{b}^{ij}\right\|^2 \qquad (22)$$

$$\left(d_\perp^i\right)^2 + \left(m_k^i - b_k^{ij}\right)^2 = \left(d_\perp^j\right)^2 + \left(m_k^j - b_k^{ij}\right)^2 \qquad (23)$$

$$b_k^{ij} = \frac{1}{2}\left[m_k^i + m_k^j + \frac{\left(d_\perp^i\right)^2 - \left(d_\perp^j\right)^2}{m_k^i - m_k^j}\right], \qquad (24)$$

where $d_\perp$ represent the distances of the cell centers (GA points) to the current conditional line, subscripts show the current axis components of the n-dimensional vectors, superscripts show the Voronoi cell index (or GA point index), and b_k^{ij} is the kth component of the boundary point b^{ij}, defined by the intersection of V_i, V_j, and the local conditional line. The method is summarized by the following steps:

[25] 1. GA: Run a classical GA, minimizing the misfit $\phi(\mathbf{m})$, save all the populations (sampled model vectors) and their likelihood values. MAP solution is obtained as the best fit model vector.

[26] 2. Voronoi decomposition and approximate PPD: Using the GA samples $\{\mathbf{m}^i\}$ and their corresponding $p(\mathbf{m}^i|\mathbf{d})$ construct the Voronoi cell structure and create the approximate PPD, $\widehat{p}(\mathbf{m}|\mathbf{d})$.

[27] 3. Gibbs resampling: Run a fast GS on the approximate PPD. No forward modeling is needed.

[28] 4. MC integral calculations: Calculate the Bayesian minimum mean square estimate (MMSE), variance and posterior distributions of desired environmental parameters, statistics for the end-user parameters, such as propagation loss L, propagation factor F, coverage diagrams, statistical radar performance prediction, such as the probability of detection and false alarm using (8)–(10), and (12) in the form of (18) as a MC integration.

[29] The accuracy of the results depends mostly on the quality of the approximate PPD, which means that, GA should gather enough samples from the entire n-dimensional search space to allow the hybrid algorithm to construct an
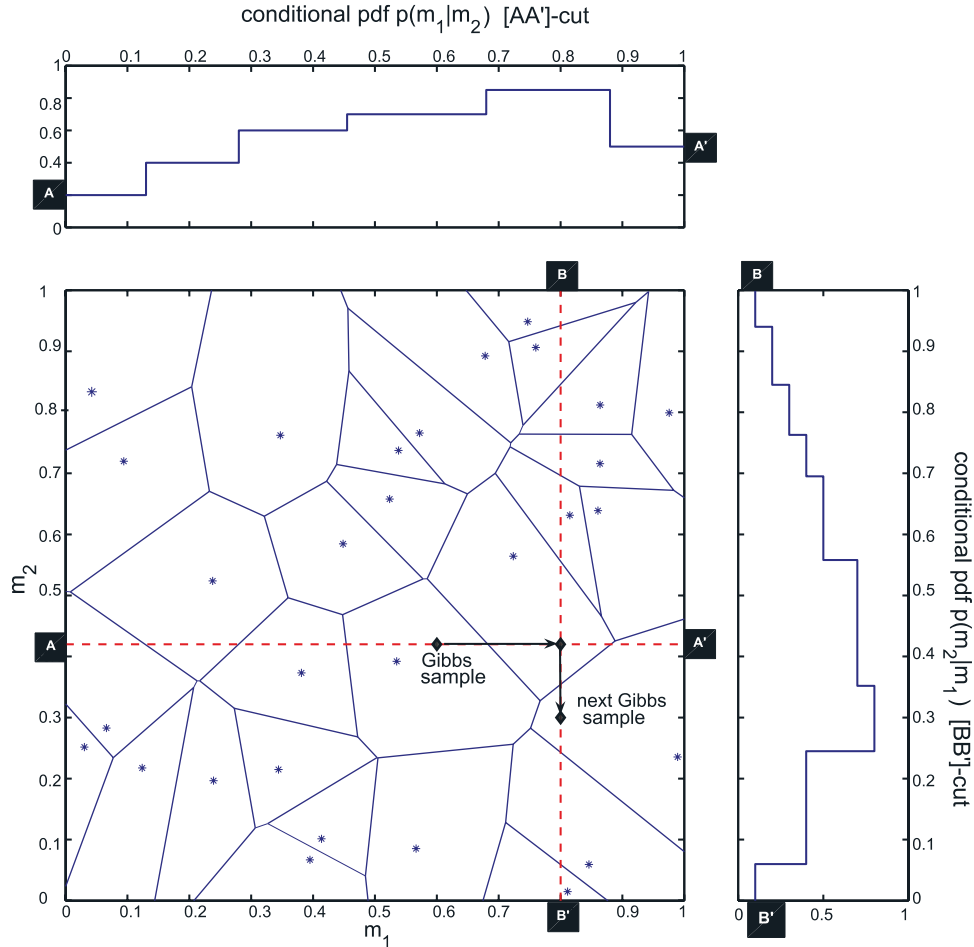
Figure 2. Voronoi cells and a single GS step for a simple two-parameter search space. Conditional PPDs used in the Gibbs step for the given conditional cut lines (AA′ and BB′) are shown on the top and to the right of the Voronoi diagram. GA and Gibbs samples are represented by asterisks and diamonds, respectively.

adequate n-dimensional mesh. Because of the approximation of the PPD, the method cannot guarantee convergence unlike MCMC samplers which are guaranteed to converge as more samples are collected.

4. Examples

4.1. Synthetic Data

[30] The method is first tested on the synthetic data given by *Yardim et al.* [2006]. In that paper, the PPD was estimated using exhaustive search, GA only, and MCMC only. Radar system and environmental parameters are given in Table 1. A typical four-parameter range-independent trilinear profile (Figure 1) is used with the unknown environment parameters and the selected upper and lower limits given in Table 2. The unknown model parameters are the slope and height of the base layer (c_1 and h_1) and the slope and thickness of the inversion layer (c_2 and h_2). Since the RFC is insensitive to the M profile parameters above the duct, the top layer slope corresponds to standard atmosphere.

[31] 1-D marginal model parameter PPDs are given in Figure 4 for exhaustive search (Figure 4a), Metropolis-Hastings sampler (conventional MCMC, Figure 4b), pure GA (Figure 4c), and hybrid GA-MCMC method (Figure 4d). Exhaustive search results are assumed to have a dense enough grid to give the true distributions and will be used as the benchmark. As expected, the Gibbs sampler results are close to the true distribution but requires 70,000 samples to converge. The GA uses 15,000 samples (5000 is enough to get the MAP
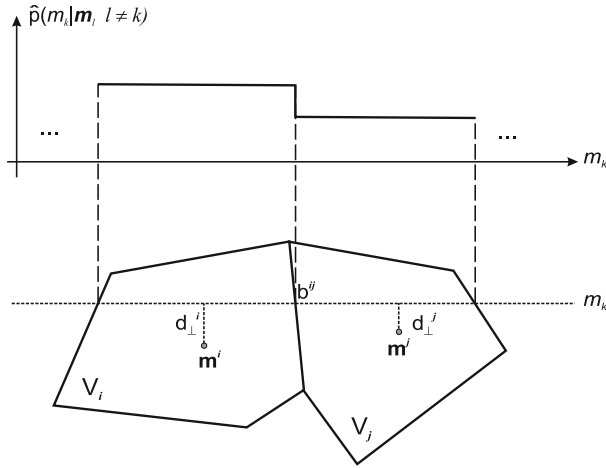
Figure 3. Two adjacent Voronoi cells V_i and V_j intersecting a conditional line in the kth dimension; $\mathbf{m}^i$ and $\mathbf{m}^j$ are the corresponding GA samples. The conditional approximate PPD, which is constant except for the cell boundary intersection, is given above the Voronoi cell structure.

solution). The distributions are clearly not accurate, however, as a global optimizer it does its job of minimizing $\phi(\mathbf{m})$ and obtaining MAP very fast. The GA sample histograms presented here are not unique. Every GA run will result in a different set of curves, without any specific sampling density $p_s(\mathbf{m}|\mathbf{d})$. The hybrid method actually uses the 15,000 GA samples

Table 1. System Parameters

Parameter	Value
Simulation	
Frequency, MHz	2840
3 dB beam width, deg	0.4
Source height, m	30.78
Polarization	VV
Duct type	SBD only
Top layer slope, M units/m	0.118
Range bin width, m	600
Environmental Model: Synthetic Data	
Number of parameters	4
M profile model type	range independent
Inversion range interval, km	10–60
Clutter standard deviation, dB	10
Environmental Model: Wallops '98 Data	
Number of parameters	16
M profile model type	range dependent
Inversion range interval, km	10–70
Ranges at which M profile is defined, km	0, 20, 40, 60

obtained in (c) to perform the Voronoi decomposition. When a fast Gibbs resampling is performed on the approximate PPD, results comparable to the conventional MCMC solution is obtained. A Gibbs resampling of just 20,000 samples is sufficient to calculate the MC integral accurately (40,000 is used in (d)). It should be noted that (d) is extracted using the forward model samples obtained in (c). All information about the search space comes from the GA samples and the hybrid method makes the information hidden in the GA set available for MC integration through Voronoi decomposition.

[32] Figures 5 provides further comparison between the benchmark exhaustive search and the hybrid method results. The off-diagonal plots are the 2-D marginal posterior densities, while 1-D parameter PPDs are given in diagonal plots. The results are given in terms of highest posterior density (HPD) regions [*Box and Tiao*, 1992]. Full Bayesian solutions in terms of posterior densities may be important in many cases and give information about the inversion quality. These marginal distributions and the interparameter correlations shown in 2-D plots may also help in understanding the underlying physics. For example the last parameter, inversion layer thickness, shows a highly non-Gaussian behavior with a high posterior probability from 15 m to 50 m. The physical explanation is that, since the selected inversion layer is very strong it will trap all of the EM signal provided that the layer has at least a certain thickness (25 m in these plots). Therefore, having an environment with a thicker inversion layer will not affect the sea clutter, so any model with $h_2 > 25$ m appears as equally likely in the plot. Hence just using the mean (MMSE) or MAP solutions may be misleading and can have significant errors. Also notice how some parameters are strongly correlated, such as the inversion layer slope c_2 and the base layer height h_1.

[33] One drawback of the hybrid method is a lack of rigorous convergence criterion. Because of its MCMC nature, the resampling converges to the sampling density. However, it is sampling the approximate density $\hat{p}(\mathbf{m}|\mathbf{d})$, not the real $p(\mathbf{m}|\mathbf{d})$. Therefore two separate conditions must be met simultaneously for the convergence of the hybrid method:

Table 2. Synthetic Data Case: Model Parameters

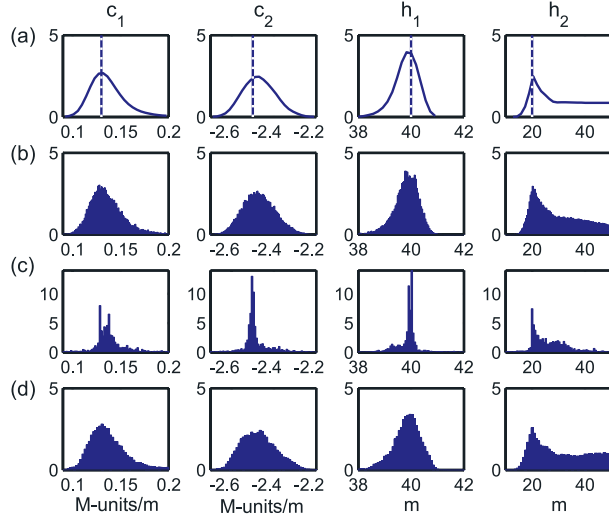| Model Parameter	Units	True Value	Lower Bound	Upper Bound
c_1	M units/m	0.13	0	0.25
c_2	M units/m	−2.5	−3.5	−1
h_1	m	40	0	50
h_2	m	20	0	50

Figure 4. Marginal posterior probability distributions for the synthetic test case. Vertical lines show the true values of the parameters. Shown are (a) exhaustive search, (b) Metropolis sampler (MCMC), (c) GA, and (d) hybrid GA-MCMC using 15,000 GA and 40,000 Gibbs samples.

[34] 1. Convergence in GA: The set of GA samples converges when $\widehat{p}(\mathbf{m}|\mathbf{d})$ obtained from the Voronoi decomposition of the GA sample set is close enough to the real PPD to yield sufficiently accurate MC integral calculations, assuming a perfect Gibbs resampling.

[35] 2. Convergence in GS: The set of Gibbs samples obtained during the resampling phase converges if the sample histograms obtained by this set is close to $\widehat{p}(\mathbf{m}|\mathbf{d})$.

[36] Hence a poor Gibbs resampling after a perfect Voronoi decomposition or a perfect Gibbs resampling on a poor Voronoi lattice may both end up with poor estimates.

[37] Figure 6 shows how the estimated 1-D marginal PPDs evolve to their true distributions with increasing GA samples for a fixed number of Gibbs samples (40,000). The metric (D) used to check the quality of the inversion result is calculated for each parameter as

$$D_j = \max_{m_j} \left| \mathrm{P}\left(m_j|\mathbf{d}\right) - \mathrm{P}_{\mathrm{TRUE}}\left(m_j|\mathbf{d}\right) \right|, \qquad (25)$$

where $\mathrm{P}(m_j|\mathbf{d})$ and $\mathrm{P}_{\mathrm{TRUE}}(m_j|\mathbf{d})$ represent the cumulative marginal distribution functions of the jth model parameter for the hybrid method and the exhaustive search result, respectively. This metric is similar to the Kolmogorov-Smirnov test statistic [*Press et al.*, 1995]. Similarly, Figure 7 explores the effect of the number of Gibbs samples in the resampling phase for a fixed

Voronoi decomposition obtained from 15,000 GA points. Note how quickly the 1-D marginals obtained by GS converge to the approximate marginal PPD (about 5000 is enough) as long as $\widehat{p}(\mathbf{m}|\mathbf{d})$ is a good Voronoi approximation to the real PPD.

[38] The convergence plots for the hybrid method are given on Figure 8. Figure 8a is obtained by performing multiple inversions using GA sample sizes varying from 10,000 to 25,000 For each GA size the inversion is repeated 40 times and the mean D value is used. Note how D improves as GA sample size is increased. Since an adequate number of Gibbs samples are used in the resampling phase, most of the error comes from the difference between the true and the approximate PPDs. Figure 8b shows the convergence in GS with different Gibbs sample sizes varying from 10,000 to 200,000. Again each simulation is repeated 40 times and the mean D is used. Given enough samples, the Gibbs sampling converges to the Voronoi-approximated PPD. Because of the inherent residual between the Voronoi approximate
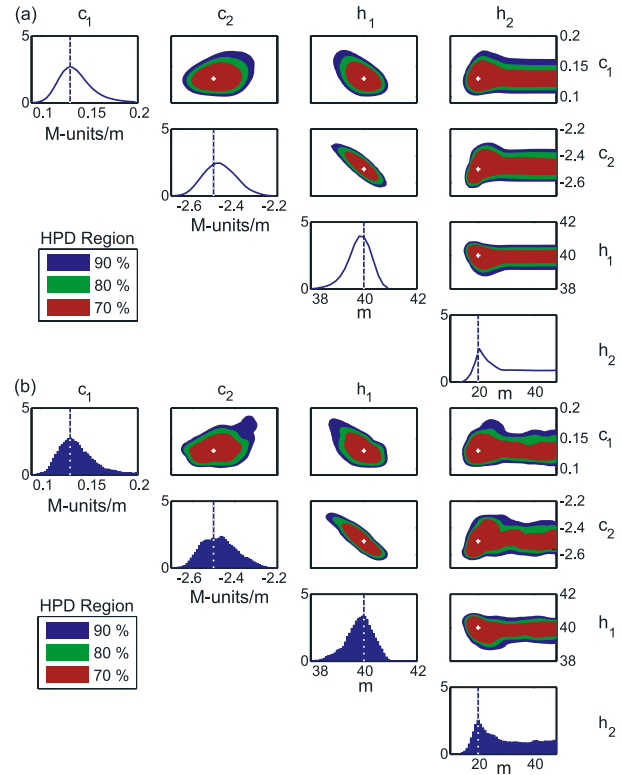

Figure 5. Both 1-D marginal (diagonal) and 2-D marginal (upper diagonal) PPDs for the synthetic test case obtained by (a) exhaustive search and (b) hybrid GA-MCMC. Vertical lines (in 1-D plots) and crosses (in 2-D plots) show the true values of the parameters.
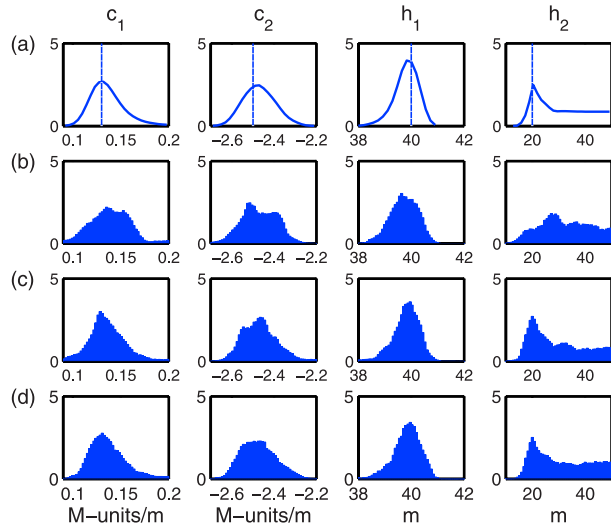
Figure 6. Convergence in GA: effect of GA sample size on 1-D marginal posterior densities for a 40,000 Gibbs sample size. Distributions were calculated using (a) exhaustive search (true distribution) and the hybrid method with (b) 1000, (c) 5000, and (d) 15,000 GA samples. Vertical lines represent the true values.

and the real PPD, increasing the GS sample size (here past about 20,000) will not improve convergence.

4.2. Wallops'98 Data

[39] To further demonstrate the capabilities and limitations of the hybrid method, a range-dependent environmental model comprising 16 parameters is employed during the inversion of the 1998 Wallops Island experiment data collected by the Naval Surface Warfare Center, Dahlgren Division. The radar clutter was gathered by the Space Range Radar (SPANDAR). Radar and environmental model parameters are both provided in Table 1. Range-dependent M profiles were measured by a helicopter provided by the Johns Hopkins University, Applied Physics Laboratory (JHU-APL). Data used in the inversion were taken during a surface-based ducting event on 2 April 1998 [*Rogers et al.*, 2000; *Gerstoft et al.*, 2003].

[40] A range-dependent inversion is achieved by defining vertical, four-parameter trilinear M profiles at certain ranges (0, 20, 40, and 60 km) and linearly interpolating the parameters in between, see Figure 9. Slopes for both the first and the second layers can be negative and positive to give more flexibility in the modeling. Hence they are only referred to by their layer numbers. Layer slopes at different ranges can vary independent of each other. On the contrary, a Markovian structure is used for the layer heights with a maximum of

30 m variation relative to the height value at the previous range.

[41] It has been shown by *Goldhirsh and Dockery* [1998] that for ranges larger than 30 km, the lateral homogeneity assumption can result in significant errors. They suggest using multiple profiles for long-range applications. In the paper by *Brooks et al.* [1999], it is suggested that a range-independent assumption for long ranges leads to significant errors in propagation factor 40% of the time and the results by *Goldhirsh and Dockery* [1998] are optimistic. Hence, in this work, a range-dependent approach with multiple profiles, each 20 km apart, is adopted. The parameters and their bounds are given in Table 3 along with the MAP solution obtained by GA. Lower and upper bounds are selected in consistency with *Rogers* [1996] and *Gossard and Strauch* [1983].

[42] Inversion results are given in Figures 10, 11, 12, and 13. Estimated range-dependent M profile (MAP solution) is given in Figure 10a. This solution is similar to the ones obtained by *Gerstoft et al.* [2003] and *Vasudevan et al.* [2007] and agrees well with the helicopter measured profile (Figure 10a. Although the helicopter profiles give a good approximation to the environment, they might not represent ground truth at the time the clutter is measured. These profiles are collected while the helicopter flies in and out radially along 150° azimuth with a sawtooth up-and-down mo-
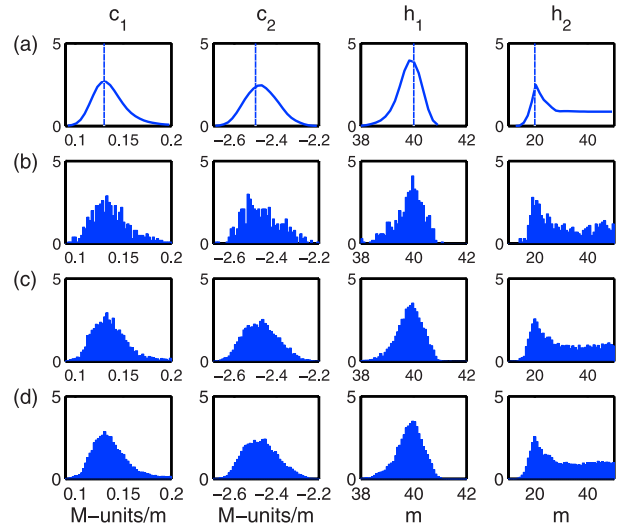

Figure 7. Convergence in GS: effect of GS sample size on 1-D marginal posterior densities for a 15,000 GA sample size. Distributions were calculated using (a) exhaustive search (true distribution) and the hybrid method with (b) 1000, (c) 5000, and (d) 20,000 Gibbs samples. Vertical lines represent the true values.
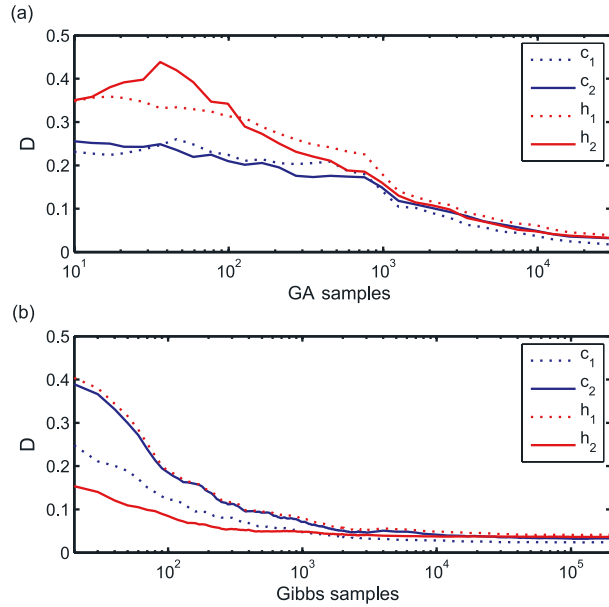
(a)

(b)

Figure 8. Convergence of the hybrid method showing D for each parameter as a function of (a) GA sample size for a 40,000 Gibbs sample size and (b) Gibbs sample size for a 15,000 GA sample size.

tion to measure the range-height-dependent refractivity. Each measurement takes about 25 min, comparable to the 30-min limit by *Rogers* [1996]. For the analyzed case the helicopter fly time is between 13:19–13:49 EST and the clutter return is measured at 13:40 EST. The sharp gradient around 60 km range disappears at the next helicopter measurement taken between 13:51–14:14 EST [see *Gerstoft et al.*, 2003, Figure 3]. So there are discrepancies between helicopter-measured and clutter-inferred profiles. In fact, the absolute mean error at 0–70 km between the helicopter and SPANDAR clutter is quite large (11.9 dB). This error value drops to 6.8 and 2.6 dB, respectively between the SPANDAR and the range-independent profile and between the SPANDAR and the range-dependent profile clutter returns. As expected, the range-dependent profile matches the relative clutter power of the SPANDAR radar (Figure 10b) better than the range-independent inversion [from *Yardim et al.*, 2006] because of the increased degrees of freedom.

[43] The environmental posterior density is given in Figure 11a. Since the full PPD is 16-D, only 1-D (diagonal plots) and 2-D (upper diagonal) marginal densities calculated using (10) are given. Some of the parameters such as m_{10}, m_{13}, and m_{14} have a highly non-Gaussian marginals, while others such as m_2, m_3, and m_9 have Gaussian-like features. The highly skewed 1-D

marginals given for m_{10} and m_{14} are encountered frequently with the refractivity slope pdfs. The reason is that the slope very rarely exceeds values such as 0.3–0.4 M units/m and usually is concentrated around values such as 0.118 M units/m (standard atmosphere) and 0.13 M units/m. This creates a sharp peak for the positive end of the spectrum since the negative slope values can be in excess of the -2 M units/m, usually with a quickly decreasing probability. The result is a pdf structure similar to the ones obtained here. In fact [*Gerstoft et al.*, 2004] use such a pdf as prior density to do importance sampling.

[44] Only 13 out of 16 parameters are given in Figure 11a. The height parameters of the second layers m_8, m_{12}, and m_{16} are omitted, as they are not important (see discussion about Figure 4. Since clutter is mostly due to the EM signal trapped inside the duct, it mostly contains information about the parameters inside the duct, making the second layer heights poorly determined except for very close ranges. To demonstrate this, normalized error function $\phi(\mathbf{m})/\phi(\mathbf{m}_{MAP})$ for various conditional planes are given in Figure 11b. These curves are obtained by fixing other parameters to their MAP values and calculating $\phi(\mathbf{m})$ while varying only two parameters at a time. Except for the bottom plots all the plots show quickly varying complex patterns whereas the last ones are flat since the horizontal axis for these is either m_8, m_{12}, or m_{16} (second layer heights). Some plots such as m_1 versus m_{12} have zero likelihood regions since the height parameters which are Δh at 20, 40, and 60 km cannot be less than values that would make the actual layer thickness negative.

[45] Therefore only 13 parameters are used in the resampling phase. This decreases computation time and reduces misleading results. For a uniformly distributed parameter the hybrid method will require much larger
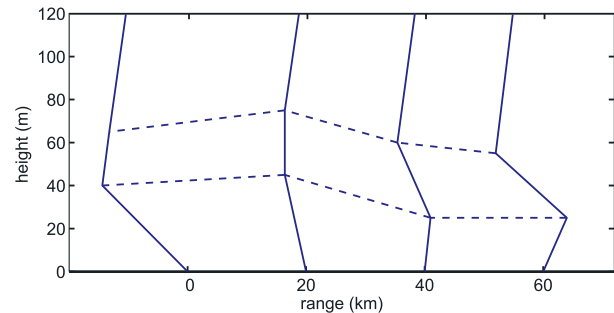

Figure 9. Example of range-dependent 16-parameter M profile with 4 parameters per 20 km. Vertical profile at any given range is calculated by linear interpolation of both the slopes and the layer thicknesses.

Table 3. Wallops'98 Experiment: Model Parameters

Model Parameter	Units	MAP Estimate	Lower Bound	Upper Bound
m_1: c_1 at 0 km	M units/m	−0.404	−2	0.4
m_2: c_2 at 0 km	M units/m	−0.721	−2	0.4
m_3: h_1 at 0 km	m	29.98	0	100
m_4: h_2 at 0 km	m	21.94	0	100
m_5: c_1 at 20 km	M units/m	−0.185	−2	0.4
m_6: c_2 at 20 km	M units/m	−0.895	−2	0.4
m_7: Δh_1 at 20 km	m	−5.03	−30	30
m_8: Δh_2 at 20 km	m	3.02	−30	30
m_9: c_1 at 40 km	M units/m	−0.391	−2	0.4
m_{10}: c_2 at 40 km	M units/m	0.060	−2	0.4
m_{11}: Δh_1 at 40 km	m	13.18	−30	30
m_{12}: Δh_2 at 40 km	m	9.94	−30	30
m_{13}: c_1 at 60 km	M units/m	−0.373	−2	0.4
m_{14}: c_2 at 60 km	M units/m	−0.098	−2	0.4
m_{15}: Δh_1 at 60 km	m	−14.25	−30	30
m_{16}: Δh_2 at 60 km	m	−14.27	−30	30

numbers of initial GA samples. This can be explained using the conditional plot of m_1 versus m_{16} in Figure 11b. Assume we have only two samples on the plane with $[m_1^1, m_{16}^1] = [−1.5 \ −20]$ and $[m_1^2, m_{16}^2] = [−0.5 \ 20]$. The

first sample m^1 has a low likelihood whereas m^2 has a much higher value, entirely due to the difference in m_1. Hence resampling after Voronoi decomposition of this sparsely sampled space will result in a nonuniform marginal for m_{16}. An interesting observation is that the other parameter m_1 is affected much less severely and indeed increasing the number of samples slightly will be enough to obtain an accurate PPD for m_1, whereas m_{16} will require much denser Voronoi cell structures. This can be problematic as the dimension size is increased. A sparse mesh will result in poor results for the uniformly distributed parameters with minimal effect on the results for other parameters. However, in RFC, because of the physics of the inversion problem, we know a priori the uniformly distributed parameters and do not include them.

[46] The environmental statistics can be projected into statistics for user parameters (see section 2). One typical parameter of interest to an end user is the propagation factor F. The results in Figure 12 are obtained from the parameter PPD in Figure 11. It shows the PPD for F at ranges 18 (Figure 11a), 40 (Figure 11b), and 60 km (Figure 11c). Contour plots show the PPD of F for height
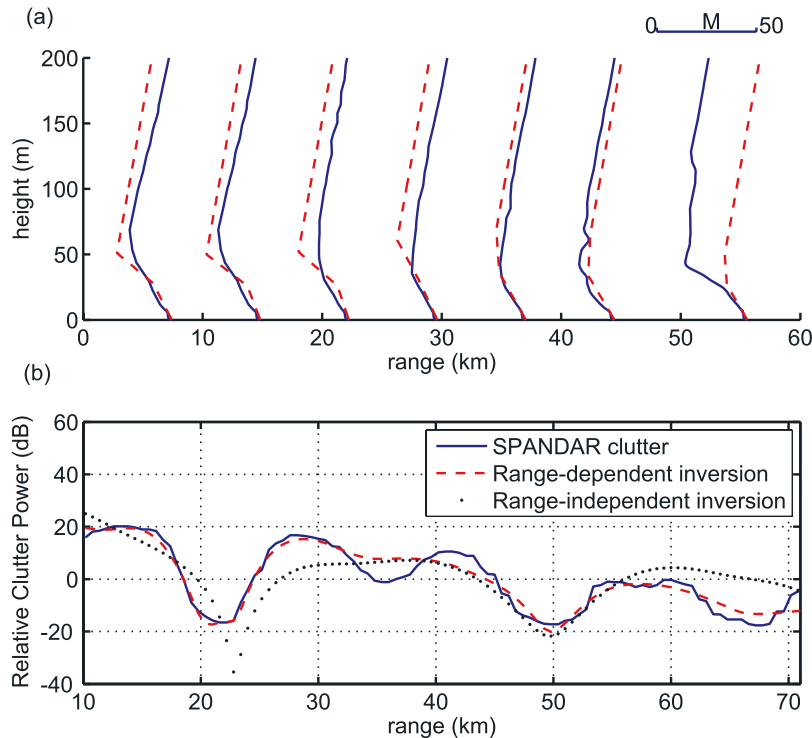

Figure 10. Inversion results for the Wallops Island experiment: (a) estimated (dashed lines) and helicopter-measured (solid lines) profiles at various ranges and (b) clutter measured by SPANDAR together with the clutter that would have been obtained from the estimated range-dependent and range-independent environments.
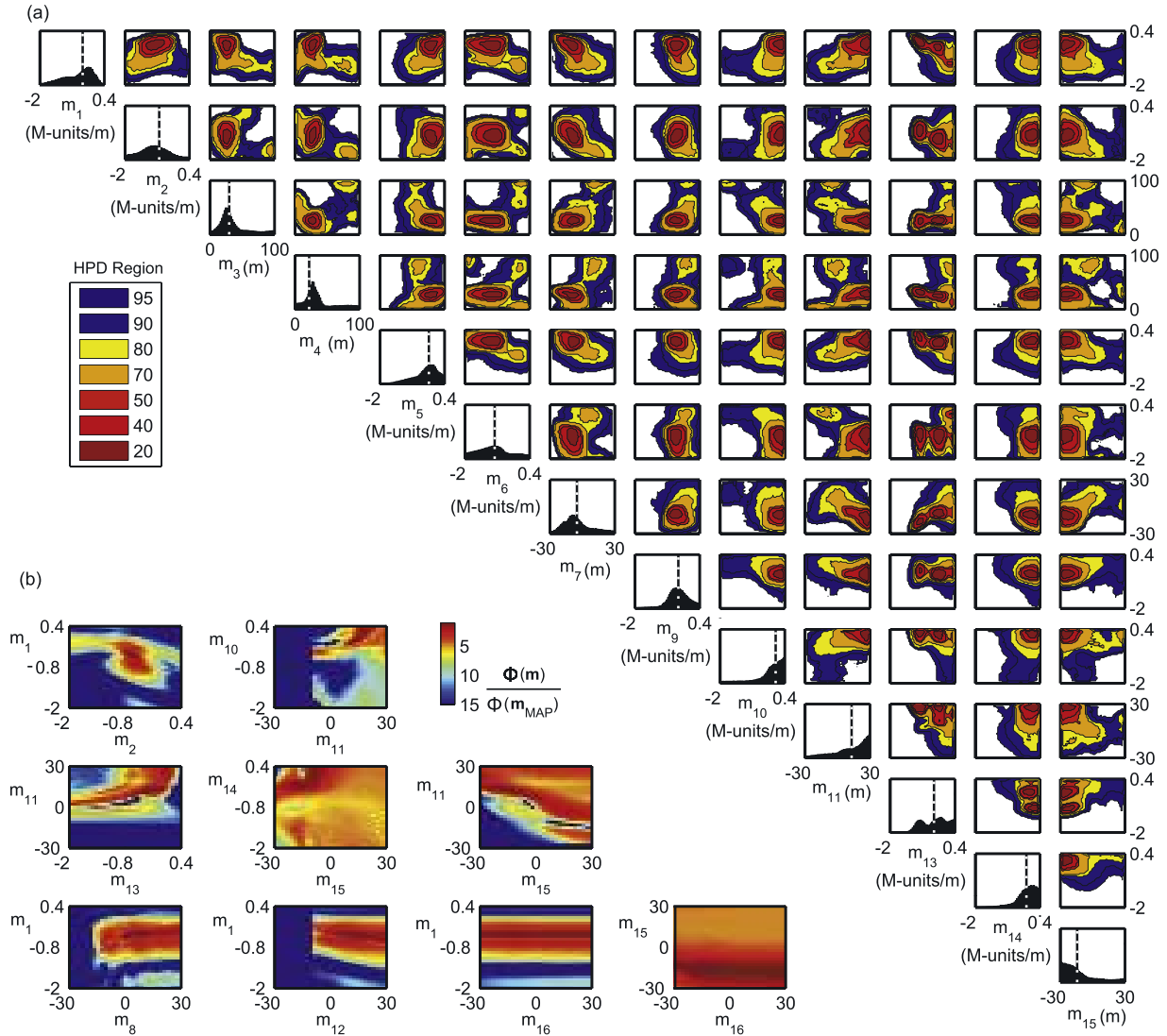
Figure 11. Marginal and conditional distributions. (a) The 1-D (diagonal) and 2-D (upper diagonal) posterior probability distributions in terms of percent HPD for the range-dependent SPANDAR data inversion. Thirteen parameters (m_{1-7}, m_{9-11}, m_{13-15}) out of 16 are given. Vertical lines in the 1-D plots show the GA MAP solution. (b) Normalized error function for various conditional planes. Each 2-D plot is obtained by fixing the other 14 parameters to their MAP values.

values between $0-200$ m, with the MAP solution (dashed white). Horizontal lines represent the three altitudes analyzed in detail in the small plots shown next to the color plots. Comparison of plots at the same range and different altitudes reveals some important aspects of RFC.

[47] First, the propagation factor PPDs inside the duct (at 20 m) are sharper than those outside the duct (100 and 180 m). This is expected since we used the sea clutter which is usually affected only by the lower portions of the atmosphere to infer the environment. The PPDs do also become flatter with increasing range. Note how the error made by using the standard atmospheric assumption (black dashed lines) increases with range, especially inside the duct. At [H, R] = [20 m, 18 km] all three curves (MAP, helicopter profile, and standard atmo-
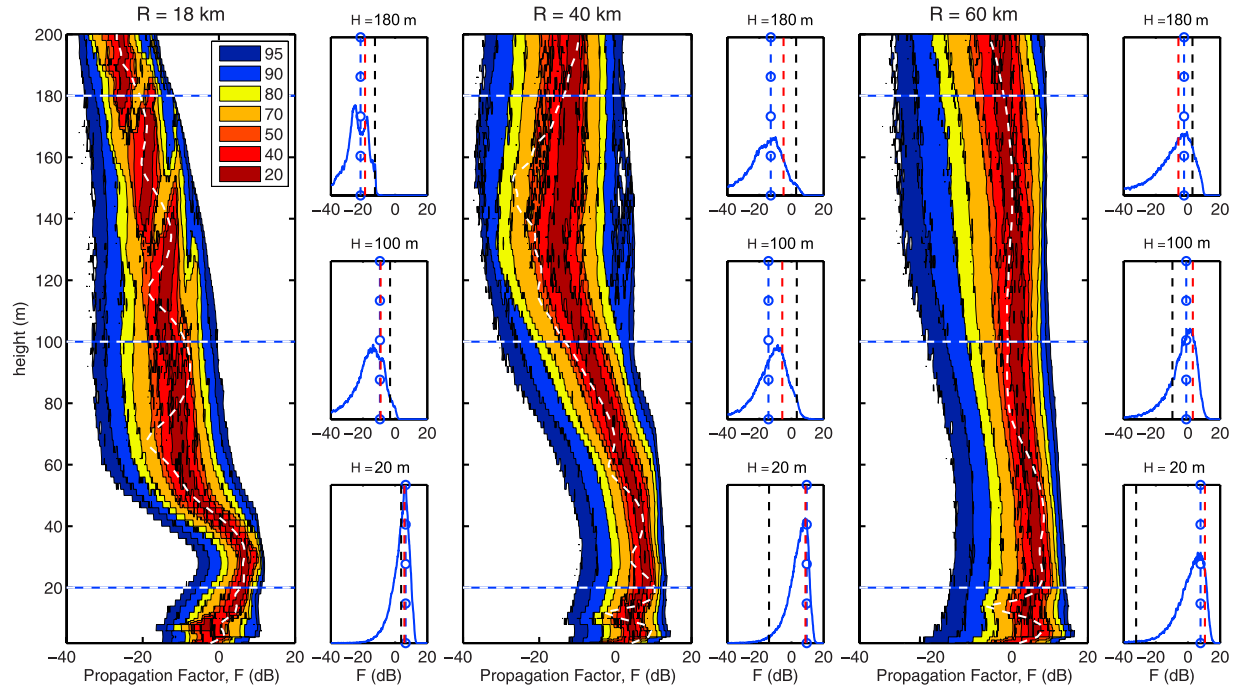
Figure 12. Posterior probability densities for propagation factor F at three different ranges: (left) 18 km, (middle) 40 km, and (right) 60 km. Color plots show the PPD of F for height values between 0 and 200 m in terms of percent HPD, with the MAP solution (dashed white lines). Horizontal lines represent the three altitudes analyzed in detail in the small plots shown next to the color plots at heights (top to bottom) 180, 100, and 20 m. Vertical lines in the small plots represent the values of F at the corresponding height and range for the MAP solution (blue line with circles), helicopter measurement (red line), and standard atmospheric assumption (black line).

sphere) are almost identical whereas standard atmospheric assumption leads to more than 40 dB error for [H, R] = [20 m, 60 km] while MAP and helicopter profile comply with the underlying PPD. Finally, the difference between the helicopter profile and MAP tends to be larger outside the duct.

[48] Similar results are obtained for F at two altitudes in Figure 13 (top) at 20 m and Figure 13 (bottom) at 100 m, inside and outside the duct, respectively. Color plots again show the PPD of F for ranges between 0 km and 90 km in terms of percent HPD, with the dashed white line showing the MAP solution. The increase in the variance of F as a function of range can clearly be seen for both inside and outside the duct cases. The variance of 100 m case is also larger than the 20 m case as also witnessed in Figure 12. It should be noted that the helicopter and MAP solution results almost always conform with the underlying density even when they are not same. Plots such as these can be used by the radar operator to update radar performance or even be included in detection algorithms as a fluctuation in the returned

signal due to the atmosphere, similar to the Swerling models [*Skolnik*, 2001].

5. Conclusion

[49] A hybrid genetic algorithm−Markov chain Monte Carlo (GA-MCMC) method has been used for statistical maritime radar performance estimation under nonstandard propagation conditions. Statistical refractivity-from-clutter (RFC) inversion is used to gather information about the environment, such as the range-dependent vertical structure of the atmospheric index of refraction, and then these environmental uncertainties are used to estimate parameters of interest to be used by the radar operator.

[50] As a forward model, a fast Fourier transform split-step parabolic equation (FFT-SSPE) approximation to the wave equation was used to propagate the electro-magnetic signal in complex environments. The hybrid method uses fewer forward model calculations than a classical MCMC while obtaining more accurate distri-
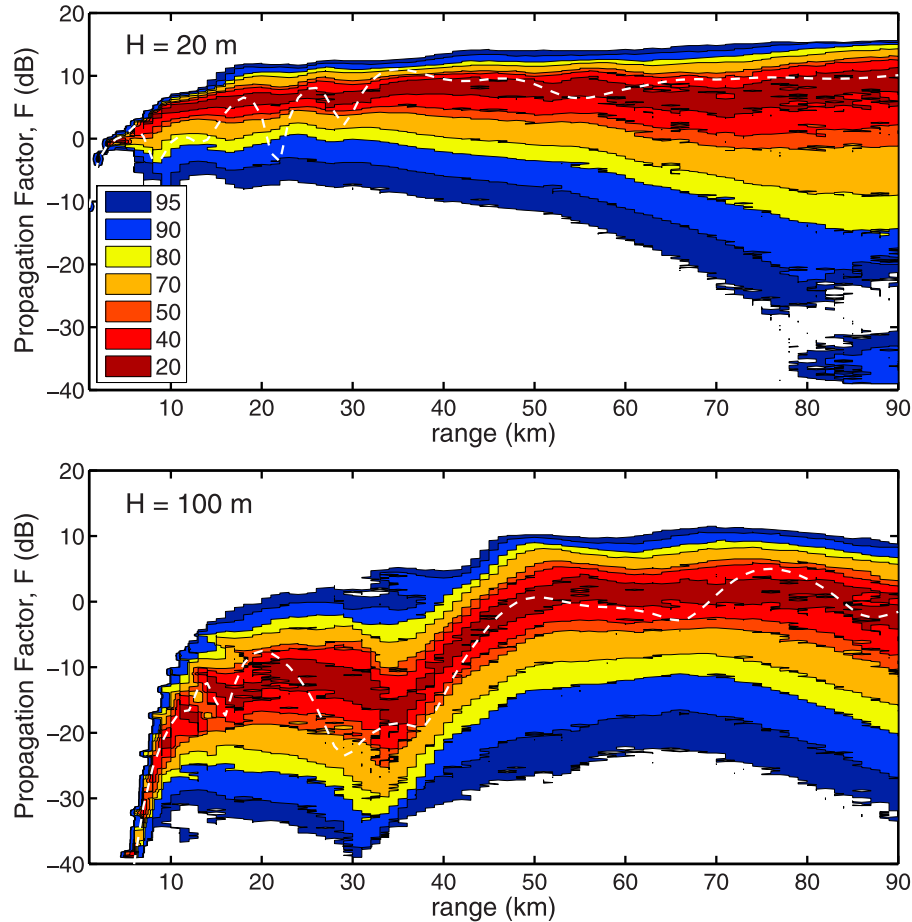
Figure 13. Posterior probability densities for propagation factor F at (top) 20 and (bottom) 100 m altitudes. Color plots show the PPD of F for ranges between 0 and 90 km in terms of percent HPD, with the dashed white line showing the MAP solution.

butions than GA. This enables inclusion of more unknown parameters and range-dependent atmospheric models. The capabilities of the technique were illustrated for a 16 dimensional range-dependent inversion.

References

Babin, S. M. (1996), Surface duct height distrubutions for Wallops Island, Virginia, 1985–1994, *J. Appl. Meteorol.*, *35*, 86–93.

Barrios, A. E. (1994), A terrain parabolic equation model for propagation in the troposphere, *IEEE Trans. Antennas Propag.*, *42*(1), 90–98.

Barrios, A. (2004), Estimation of surface-based duct parameters from surface clutter using a ray trace approach, *Radio Sci.*, *39*, RS6013, doi:10.1029/2003RS002930.

Box, G. E. P., and G. C. Tiao (1992), *Bayesian Inference in Statistical Analysis*, Addison-Wesley, New York.

Brooks, I. M., A. K. Goroch, and D. P. Rogers (1999), Observations of strong suface radar ducts over the Persian Gulf, *J. Appl. Meteorol.*, *38*, 1293–1310.

Cook, J., and S. Burk (1992), Potential refractivity as a similarity variable, *Boundary Layer Meteorol.*, *58*(1–2), 151–159.

Geman, S., and D. Geman (1984), Stochastic relaxation, Gibbs distributions, and the Bayesian restoration of images, *IEEE Trans. Pattern Anal. Machine Intel.*, *6*, 721–741.

Gerstoft, P., L. T. Rogers, J. L. Krolik, and W. S. Hodgkiss (2003), Inversion for refractivity parameters from radar sea clutter, *Radio Sci.*, *38*(3), 8053, doi:10.1029/2002RS002640.

Gerstoft, P., W. S. Hodgkiss, L. T. Rogers, and M. Jablecki (2004), Probability distribution of low-altitude propagation loss from radar sea clutter data, *Radio Sci.*, *39*, RS6006, doi:10.1029/2004RS003077.

Goldhirsh, J., and D. Dockery (1998), Propagation factor errors due to the assumption of lateral homogenity, *Radio Sci.*, *33*(2), 239–249.

Gossard, E. E., and R. G. Strauch (1983), *Radar Observations of Clear Air and Clouds*, Elsevier, New York.

Hastings, W. (1970), Monte Carlo sampling methods using Markov chains and their applications, *Biometrika*, *57*, 97–109.

Hodur, R. M. (1996), The naval research laboratory's coupled ocean/atmosphere mesoscale prediction system (COAMPS), *Mon. Weather Review*, *125*(7), 1414–1430.

Huang, C.-F., P. Gerstoft, and W. S. Hodgkiss (2006), Validation of statistical estimation of transmission loss in the presence of geoacoustic inversion uncertainty, *J. Acoust. Soc. Am.*, *120*(4), 1932–1941.

Jeske, H. (1973), State and limits of prediction methods of radar wave propagation conditions over the sea, in *Modern Topics in Microwave Propagation and Air-Sea Interaction*, *NATO ASI Ser., Ser. C*, vol. 5, edited by A. Zancla, pp. 130–148, NATO Adv. Study Inst., Sorrento, Italy.

Levy, M. (2000), *Parabolic Equation Methods for Electromagnetic Wave Propagation*, Inst. of Electr. Eng., London, U. K.

Liu, W. T., K. B. Katsaros, and J. A. Businger (1979), Bulk parameterization of air-sea exchanges of heat and water vapor including the molecular constraints at the interface, *J. Atmos. Sci.*, *36*, 1722–1735.

MacKay, D. J. C. (2003), *Information Theory, Inference and Learning Algorithms*, Cambridge Univ. Press, Cambridge, U. K.

Metropolis, N., A. W. Rosenbluth, M. N. Rosenbluth, A. H. Teller, and E. Teller (1953), Equation of state calculations by fast computing machines, *J. Chem. Phys.*, *21*, 1087–1092.

Okabe, A., B. Boots, K. Sugihara, and S. N. Chiu (2000), *Spatial Tessellations—Concepts and Applications of Voronoi Diagrams*, 2nd ed., John Wiley, New York.

Ó Ruanaidh, J. J. K., and W. J. Fitzgerald (1996), *Numerical Bayesian Methods Applied to Signal Processing, Stat. and Comput. Ser.*, Springer, New York.

Paulus, R. A. (1985), Practical application of an evaporation duct model, *Radio Sci.*, *20*(4), 887–896.

Press, W. H., S. A. Teukolsky, W. T. Vetterling, and B. Flannery (1995), *Numerical Recipes in C*, 2nd ed., Cambridge Univ. Press, Cambridge, U. K.

Rogers, L. T. (1996), Effects of variability of atmospheric refractivity on propagation estimates, *IEEE Trans. Antennas Propag.*, *44*(4), 460–465.

Rogers, L. T., C. P. Hattan, and J. K. Stapleton (2000), Estimating evaporation duct heights from radar sea echo, *Radio Sci.*, *35*(4), 955–966.

Rogers, L. T., M. Jablecki, and P. Gerstoft (2005), Posterior distributions of a statistic of propagation loss inferred from radar sea clutter, *Radio Sci.*, *40*, RS6005, doi:10.1029/2004RS003112.

Rowland, J. R., and S. M. Babin (1987), Fine-scale measurements of microwave profiles with helicopter and low cost rocket probes, *Johns Hopkins APL Tech. Dig.*, *8*(4), 413–417.

Sambridge, M. (1999a), Goephysical inversion with a neighborhood algorithm—I. Searching a parameter space, *Geophys. J. Int.*, *138*, 479–494.

Sambridge, M. (1999b), Geophysical inversion with a neighborhood algorithm—II. Appraising the ensemble, *Geophys. J. Int.*, *138*, 727–746.

Sambridge, M. (2001), Finding acceptable models in nonlinear inverse problems using a neighbourhood algorithm, *Inverse Probl.*, *17*, 387–403.

Sambridge, M. (2003), An ensemble view of Earth's inner core, *Science*, *299*(5606), 529–530.

Skolnik, M. I. (2001), *Introduction to Radar Systems*, 3rd ed., McGraw-Hill, New York.

Thews, E. R. (1990), Timely prediction of low-altitude radar performance in operational environments using in situ atmospheric refractivity data, *IEE Proc., Part F*, *137*(2), 89–94.

Vasudevan, S., R. H. Anderson, S. Kraut, P. Gerstoft, L. T. Rogers, and J. L. Krolik (2007), Recursive Bayesian electromagnetic refractivity estimation from radar sea clutter, *Radio Sci.*, *42*, RS2014, doi:10.1029/2005RS003423.

Voronoi, G. (1908), Nouvelles applications des paramètres continus à la théorie des formes quadratiques, *J. Reine Angew. Math.*, *133*, 97–178.

Yardim, C., P. Gerstoft, and W. S. Hodgkiss (2006), Estimation of radio refractivity from radar clutter using Bayesian Monte Carlo analysis, *IEEE Trans. Antennas Propag.*, *54*(4), 1318–1327.

————————

P. Gerstoft, W. S. Hodgkiss, and C. Yardim, Marine Physical Laboratory, University of California, San Diego, La Jolla, CA 92037–0238, USA. (gerstoft@ucsd.edu; whodgkiss@ucsd.edu; cyardim@ucsd.edu)